Surface Plasmon Dependence on the Electron Density Profile at Metal Surfaces

Christin David[†,‡] and F. Javier García de Abajo[‡,§,*]

[†]IQFR-CSIC, Serrano 119, 28006 Madrid, Spain, [‡]ICFO-Institut de Ciencies Fotoniques, Mediterranean Technology Park, 08860 Castelldefels (Barcelona), Spain, and [§]ICREA-Institució Catalana de Recerca i Estudis Avançats, Passeig Lluís Companys, 23, 08010 Barcelona, Spain

ABSTRACT We use an extension of the hydrodynamic model to study nonlocal effects in the collective plasmon excitations at metal surfaces and narrow gaps between metals, including the surface spill-out of conduction band electrons. In particular, we simulate metal surfaces consisting of a smooth conduction-electron density profile and an abrupt jellium edge. We focus on aluminum and gold as prototypical examples of simple and noble metals, respectively. Our calculations agree with the dispersion relations measured from planar surfaces for these materials. Systems involving small gaps display a regime of tunnelling electrons, which is partially captured by the overlap of electron densities. This extension of the hydrodynamic model to cope with inhomogeneous density profiles provides a relatively fast and accurate way of describing the optical response of metal surfaces at subnanometer distances.

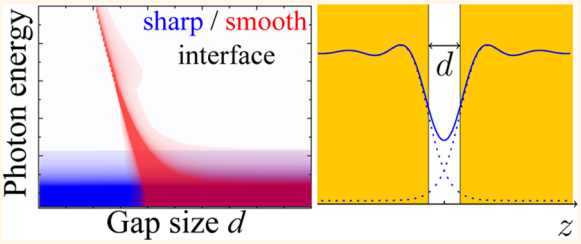

KEYWORDS: plasmons · nonlocal effects · hydrodynamic model · smooth density profile · spatial dispersion

Plasmons, the collective excitations sustained by conduction electrons at metal surfaces, possess a number of properties that make them attractive for nanoscience:[1] they provide a robust way of strongly coupling light to nanometer-sized structures, where they can be localized, giving rise to high electric-field intensities, which can be orders of magnitude larger than the externally applied light intensity.[2] Additionally, plasmons can be tuned in frequency and spatial distribution through varying the surface geometry and environment.[3] In particular, the sensitivity to the environment is routinely used for detecting the presence of minute amounts of analytes.[4] Recent advances in nanofabrication are pushing plasmons to extreme levels of confinement and field enhancement, particularly by exploiting the gap between two neighboring metal surfaces. For example, colloid synthesis can produce gaps between two metal nanoparticles of fixed subnanometer separation by using molecular binders such as dithiols[5] (self-assembly bottom-up approach). Also, top-down lithographic methods provide a higher degree of control over larger structures. The combined use of metal-colloids assembly on lithographic structures enables the simultaneous control over large-scale areas and the size of narrow gaps at designated positions. Alternatively, nanoprobes are used to hold metal surfaces at subnanometer distances.[6,7] The extreme properties of plasmons in narrow gaps have been widely used for sensing[4,8] and nanoscale nonlinear optics,[6] but the number of applications in nanophotonics keeps on increasing.

Molecular sensing constitutes a primary example of application of the strong optical field enhancement associated with localized plasmons. Single-molecule detection and chemical determination are made possible by this localization using for example surface-enhanced Raman scattering (SERS).[9] Gold is commonly employed in these studies, as it is chemically inert and displays surface plasmons in the visible and near-infrared (vis–NIR) parts of the spectrum, depending on geometry.[10] In particular, nanometer-sized point-like gaps flanked by metal surfaces favor the formation of hotspots that can produce amplification of the externally applied light intensity by over 5 orders of magnitude.[9] The relevance of these geometries for sensing

* Address correspondence to javier.garciadeabajo@icfo.es.

Received for review July 15, 2014 and accepted August 19, 2014.

Published online August 19, 2014
10.1021/nn5038527

© 2014 American Chemical Society

has prompted a large deal of work aimed at exploring their optical performance.[11−13] A strong redshift is observed as the two metal surfaces are brought closer together. Remarkably, classical electromagnetism based upon the use of local dielectric functions for the involved materials provides an accurate level of description down to gap distances ∼1−2 nm in noble metals. However, as many molecules of interest are subnanometer in size, their interaction with metal surfaces requires going beyond classical local theory, so one is faced with nonlocality, in addition to the surface spill-out of valence electrons,[14−17] originating in their wave nature. In this context, planar surfaces have been studied for a long time,[18] starting from the specular-reflection model,[19−24] which predicts a nonlocal dispersion of the surface plasmons. The semiclassical hydrodynamic model has been shown to lead to similar effects by incorporating the quantum nature of valence electrons through the hydrodynamic pressure of the noninteracting homogeneous electron gas.[24−29] Density-functional theory (DFT), particularly in the local density approximation (LDA),[15,17] has resulted in the prediction of plasmon-frequency redshifts caused by the smaller electron density at the surface spill-out region in simple metals.[14] This effect is accompanied by weaker *d*-band screening in noble metals, in which the net result is a surface plasmon blue shift.[14] Similar blue shifts are also observed in metal nanoparticles,[11,13] accompanied by plasmon broadening that can be phenomenologically described within an electron confinement picture,[30] while a recent theoretical development based upon nonlocal response offers an alternative explanation of this effect.[31]

The analysis of the gap geometry is more complex. Recent studies of tips in close proximity have shown the presence of spectral features that are missed by classical theory at gap distances below ∼1 nm.[7,17] The plasmon redshift associated with the interaction across the gap, as derived from classical theory, becomes a blue shift at gap separations ∼0.5 nm,[15] as confirmed by experiment.[7,12,13] Additionally, nonlocal effects have been shown to cause a reduction in field enhancement,[23,27] which is consistent with recent experimental observations.[12] While a detailed first-principles analysis of the gap geometry is still missing due to the numerical complexity of the problem, simplified approaches have been followed such as the DFT-LDA within a jellium model, which has been pioneered for planar surfaces[14] and recently used to investigate curved morphologies including gaps.[7,15−17,32]

The need for fast numerical methods that are capable of dealing with complex geometries has stimulated computational research based upon the Bloch hydrodynamic model,[25] following a long series of plasmonics studies.[26−29] This model has been used to investigate nonlocal effects in a variety of geometries.[27,33−43] Its simplicity allows us to derive analytical expressions in simple shapes, such as the nonlocal Mie coefficients of homogeneous and coated spheres with inclusion of retardation effects.[27] Upon the basis of the use of a single parameter (the hydrodynamic pressure coefficient β), this model successfully predicts a reduction of field enhancement, as well as weaker plasmon-hybridization redshifts.[27,37,40] However, its main drawback lies in the fact that surfaces and interfaces are described as abrupt boundaries. Although this type of description is widely and successfully used in classical electrodynamics modeling of plasmonics, the effects of electron spill-out cannot be ignored at short distances, where the abrupt interface assumption is a severe approximation considering that the conduction electron density profile extends ∼0.2 nm outside the surface,[44] therefore totaling a significant fraction of the gap for subnanometer separations.

In this work, we use an extension of the hydrodynamic model that allows us to deal with smooth electron density profiles, following previous studies of this formalism for plasmons in planar surfaces[45] and second harmonic response.[46] Eguiluz *et al.*[45] presented the fundamentals of this model and used it to predict additional multipolar plasmon modes in sufficiently diffused interfaces. Here, we study the effect of electron spill-out on the surface plasmons of simple geometries that are relevant for plasmonics applications, such as planar surfaces, narrow gaps, and thin films, using realistic DFT-LDA density profiles obtained from the jellium model for gold and aluminum[44] (see Figure S2a in the SI), assuming a local variation of the hydrodynamic pressure coefficient β, as well as a sharp edge of the *d*-band screening background. We find agreement with available experiments for planar surfaces, as well as a strong influence of the density profiles when comparing sharp and smooth boundaries: the effects of electron spill-out are generally dominant with respect to those originating in a finite hydrodynamic pressure.

RESULTS AND DISCUSSION

Inhomogeneous Hydrodynamic Model. It is instructive to briefly revise the fundamentals of the hydrodynamic model, in which the optical response of a nanostructured metal is described in terms of a continuous bounded electron gas that evolves according to the hydrodynamic Euler equation[25,45,46]

$$n(\partial/\partial t + \gamma + \mathbf{v}\cdot\nabla)m_e\mathbf{v} = -\nabla p - en\mathbf{E} \qquad (1)$$

where n is the conduction electron density, $\mathbf{v}$ is the electron velocity, γ is an intrinsic inelastic damping rate, p is the hydrodynamic pressure, and $\mathbf{E}$ is the total electric field. We work in the electrostatic limit and assume linear response, so that the disturbance in the induced electron density $n - n_0$ is small compared with the unperturbed position-dependent density n_0 (see Figure S3 in the Supporting Information, SI). In the unperturbed system, $p = p_0$ is the static hydrodynamic

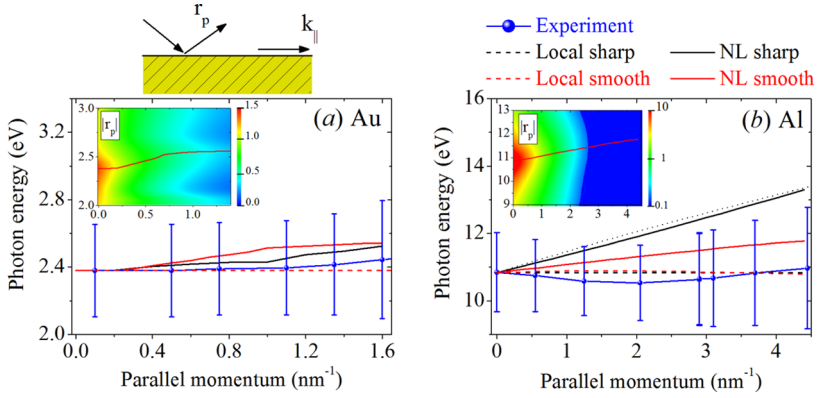

Figure 1. Surface plasmon dispersion in gold and aluminum. We present results obtained from different models for the surface plasmon dispersion relation (see upper right legend), as compared with experimental data (symbols) for (a) gold[10] and (b) aluminum.[51] The insets show the calculated reflection coefficient $|r_p|$ as obtained from the nonlocal (NL) smooth-profile model. The small $k_\parallel$ analytical limit of the NL sharp model is shown as a dotted line in (b).

pressure, which according to eq 1 has to compensate the static field $\mathbf{E}_0 = -(\nabla p_0)/en_0$ produced by both n_0 and the background jellium density.[45] In practice, we adopt the classical Thomas–Fermi model to obtain a local approximation to the pressure from the variation of the kinetic energy of a noninteracting electron gas with respect to volume.[47] This yields $p = [9(3\pi^2)^{2/3}\hbar^2/25m_e]n^{5/3}$. A factor of 9/5 is added to this expression in order to account for electron–electron Coulomb interaction, which leads to a low-momentum bulk plasmon dispersion that agrees with the Lindhard formula.[48,49] Now, neglecting higher-order terms in eq 1 beyond linear response, and focusing on monochromatic components of frequency ω, we find

$$i(\omega + i\gamma)\mathbf{j}^{\text{ind}} = \beta^3\nabla\left(\frac{\rho^{\text{ind}}}{\beta}\right) + \frac{e^2n_0}{m_e}\nabla\phi \qquad (2)$$

where $\beta = (3/5)^{1/2}v_F$, $v_F = (\hbar/m_e)(3\pi^2n_0)^{1/3}$ is the Fermi velocity, and we have defined the induced electron current and density as $\mathbf{j}^{\text{ind}} = -en_0\mathbf{v}$ and $\rho^{\text{ind}} = -e(n - n_0)$, as well as the induced scalar potential ϕ (*i.e.*, $\mathbf{E} - \mathbf{E}_0 = -\nabla\phi$). Equation 2 has to be self-consistently solved together with the continuity equation

$$\nabla\cdot\mathbf{j}^{\text{ind}} = i\omega\rho^{\text{ind}} \qquad (3)$$

and Poisson's equation

$$\nabla\cdot\epsilon_b\nabla\phi = -4\pi\rho^{\text{ind}} \qquad (4)$$

where we have defined ϵ_b as a background permittivity, which arises from interband transitions and core polarization, and we set it in practice to an ω-dependent complex value leading to a bulk dielectric function that matches measured data[50] (see Figure S1 in the SI). This is particularly important in noble metals (*e.g.*, $\epsilon_b \approx 9$ for gold). For bounded media, we assume this value of ϵ_b inside the jellium, whereas we take $\epsilon_b = 1$ outside (see Methods). This adds a sharp dielectric background edge, which requires imposing the continuity of ϕ and $\epsilon_b\partial_\perp\phi$, where $\partial_\perp$ denotes the normal derivative, in order to avoid unphysical divergences in eq 4. Likewise, eq 3 leads to the continuity of the current $\mathbf{j}^{\text{ind}}$, whereas eq 2 imposes the continuity of ρ^{ind}/β.

In this paper, we apply this model to study the effect of nonabrupt electron density profiles at planar metal surfaces, gaps, and thin films. We need to solve the above equations for systems that are translationally invariant along the surface directions and present z-dependent profiles. The reflection and transmission coefficients of those structures are obtained using a transfer-matrix approach for each fixed value of the parallel wave vector $k_\parallel$. More precisely, we describe the structure as a concatenation of thin homogeneous layers that are connected *via* the boundary conditions noted above (see Methods for a detailed derivation). This model is supplemented with measured optical data for the metal dielectric function $\epsilon_\perp(\omega)$ (see eq 7). In particular, we extract the background permittivity ϵ_b for gold[50] by subtracting a Drude term from $\epsilon_\perp(\omega)$ with bulk plasmon energy $\hbar\omega_p = 8.9$ eV and width $\hbar\gamma = 0.071$ eV (see Figure S1 in the SI). For aluminum, the dielectric function is well reproduced with $\epsilon_b = 1$ (*i.e.*, negligible deeper band screening), $\hbar\omega_p = 15.3$ eV, and $\hbar\gamma = 0.5$ eV. In what follows, we compare the model presented above (*NL smooth*) with its local $\beta \to 0$ limit (*local smooth*), as well as with results obtained by sharpening the surface profile to a step function (*NL sharp* and *local sharp* analytical models). The latter correspond to hydrodynamic approaches presented in the literature.[25−29,33−43]

Plasmons in Single Metal Surfaces. We first examine the role of the electron density profile on the plasmons of a semi-infinite metal. The plasmon resonance frequency is obtained for each $k_\parallel$ from the maximum of the reflection coefficient, which we calculate according to eq 15 (see Methods and insets of Figure 1). Results for gold and aluminum are presented in Figure 1a and Figure 1b, respectively. All four models (*i.e.*, local and nonlocal with either smooth or sharp density profiles)

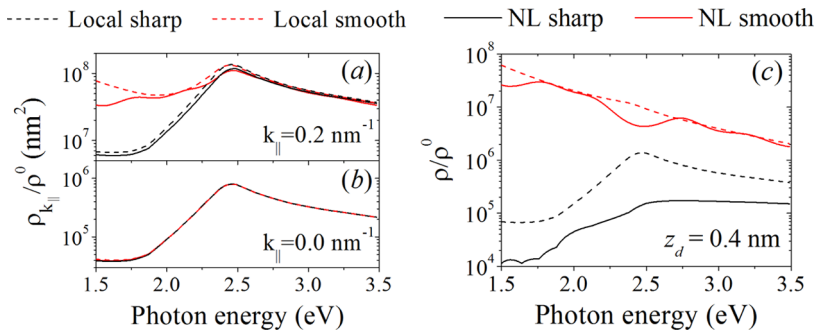

Figure 2. Local density of optical states (LDOS) near a gold surface. (a,b) Spectral dependence of selected $k_\parallel$ contributions to the LDOS. (c) Full LDOS obtained upon integration over $k_\parallel$. Different models are considered, as shown in the upper legend. The LDOS is calculated at a distance $z_d = 0.4$ nm relative to the jellium edge and normalized to the projected free-space LDOS $\rho^0 = \omega^2/3\pi^2c^3$.

produce relatively flat dispersion relations in gold, in agreement with experiment.[10] Incidentally, the position of the *d*-band screening edge (*i.e.*, the boundary between bulk $\epsilon_b \neq 1$ and vacuum $\epsilon_b = 1$) is taken at the jellium edge, assuming (111) surface orientation (see SI). Interestingly, the NL sharp model is in clear disagreement with experiment for aluminum,[51] whereas the other models lead again to relatively dispersionless profiles. The numerical result for the NL sharp model is further corroborated by comparison with its analytical small $k_\parallel$ limit[19,45,52] $\omega = \omega_p/(2)^{1/2} + \beta k_\parallel/2$ for A1 ($\epsilon_b = 1$), shown as a dotted line in Figure 1b.

As we are interested in small distances, where the effects of nonlocality and the smooth density profile are more important, we examine next the local density of optical states (LDOS), which corresponds to the sum of the electric field intensity for all normalized optical modes at a given position and frequency.[53] This quantity is uniquely defined in nonabsorbing media, where it is simply proportional to the imaginary part of the self-induced electric field at the position and along the direction of a point dipole source.[54] In particular, it takes the value $\rho^0 = \omega^2/3\pi^2c^3$ in free space. In lossy media, we can still generalize this concept through an *ad hoc* definition of the LDOS as the noted imaginary part of the induced field. This definition coincides with the true LDOS in nonabsorbing media but it is only an artificial tool to investigate plasmon dispersion relations in the interior of lossy materials. Details on its calculation in the present smooth profile formalism are given in the Methods section, where we also define its parallel-wave-vector decomposition $\rho_{k_\parallel}$. We focus for simplicity on the LDOS component along the *z* direction, normal to the surface.

The LDOS near a gold surface is discussed in Figure 2 at a distance $z_d = 0.4$ nm from the jellium edge. The $k_\parallel$-resolved LDOS coincides in all four models for $k_\parallel = 0$ (Figure 2b), as this limit effectively corresponds to large distances with respect to the surface (*e.g.*, the dipole field from which the LDOS is calculated decays as $\exp(-k_\parallel z_d)$), so that the detailed variation of the density profile is not resolved. In contrast, the results depend on the model for finite $k_\parallel$ (Figure 2a). Importantly, larger variations are observed between sharp- and smooth-profile models than between local and NL models. We thus have a first indication that a proper account of the smooth variation in the electron density profile is more relevant at short distances than bulk spatial dispersion through the parameter β. A similar conclusion is obtained from the $k_\parallel$-integrated LDOS (Figure 2c). Incidentally, except in the unrealistic local sharp model, the LDOS spectra are rather featureless, indicating that the surface-plasmon resonance that is otherwise observed in far-field reflection (see inset to Figure 1a) is attenuated by the contribution of high $k_\parallel$ components when examining the near-the-surface response.

Gap Plasmons. The features in the $k_\parallel$-resolved LDOS of a gap between two metal surfaces allows us to characterize plasmons in this geometry. We show in Figure 3 results for a gold gap (jellium-to-jellium distances $d = 0.5$ and 1 nm) and observe again a strong variation when moving from a sharp to a smooth density profile, whereas the effect of finite hydrodynamic pressure (*i.e.*, β) is relatively smaller. At distances of a few nanometers, all four models converge to similar dispersion relations (see Figure S4 in the SI), but for the distances shown in Figure 3, the discrepancies are striking. Smooth profiles basically displace the spectral weight toward lower frequencies compared to sharp profiles, also resulting in broader features. The NL sharp model (Figure 3a,e) produces less pronounced redshifts and broadening compared to the local sharp model (Figure 3c,g), as previously described in the literature,[23] but these changes are minor compared to the effect produced by electron spill-out. Profile smoothing also leads to a number of low-energy features when combined with finite β (Figure 3d,h). We show the gap LDOS as a function of gap distance in Figure 4. The results are consistent with the conclusions extracted from Figure 3 by comparing different models. For smooth profiles, which should be considered as a more realistic description than sharp interfaces, the spectra are dominated by low-energy features that are blue-shifted with decreasing gap

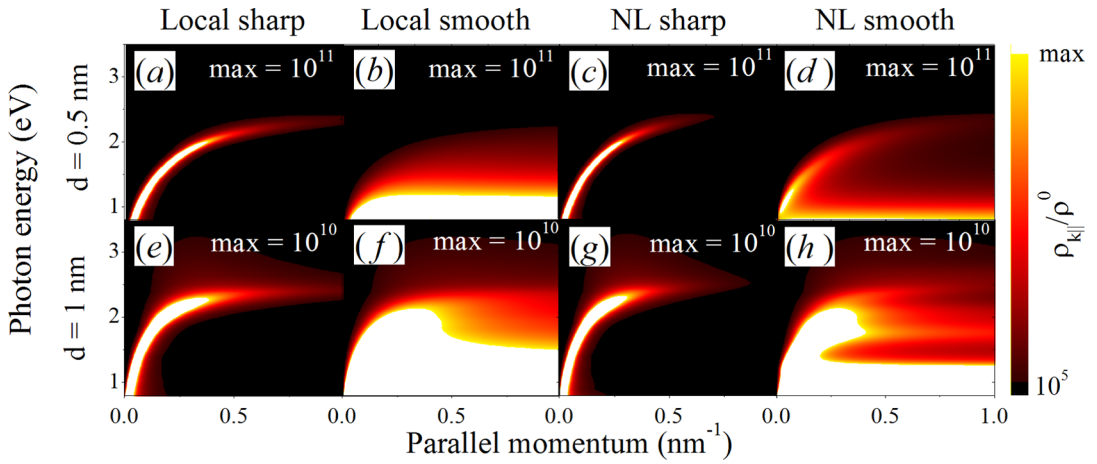

Figure 3. Plasmon dispersion relation in the gap between two gold surfaces. We represent the $k_{\parallel}$ and energy dependence of the LDOS at the gap center for separations (a–d) d = 0.5 nm and (e–h) d = 1 nm (see Figure 7b). Different models for the response are considered, as indicated in the upper labels.

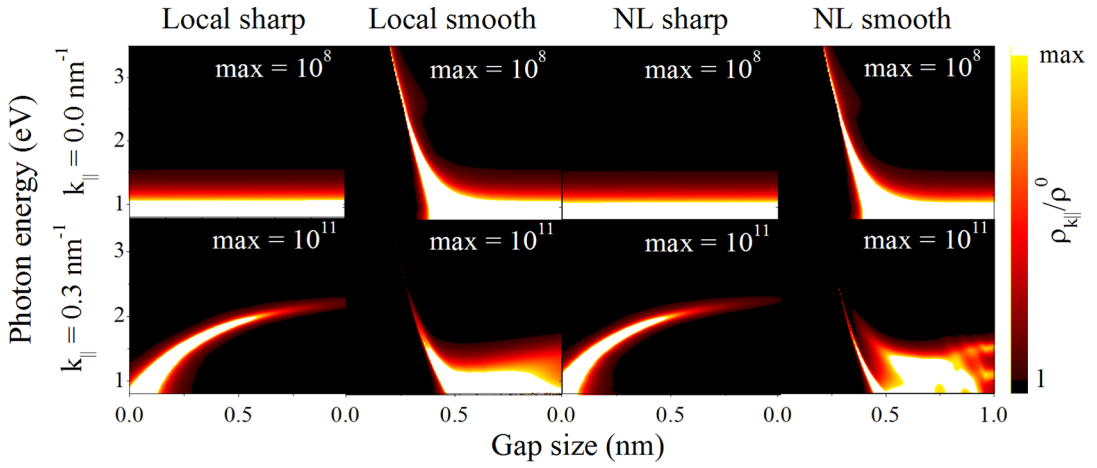

Figure 4. Gap plasmon dependence on gap size. We represent the LDOS at the gap center as a function of gap size d and photon energy for both $k_{\parallel}$ = 0 (upper plots) and $k_{\parallel}$ = 0.3 nm^{-1} (lower plots) using different response models for gold (see upper labels).

distance, in clear contrast to what happens for sharp surfaces.

The $k_{\parallel}$ dependence of the plasmon energy in the planar gap geometry can be used to obtain the gap plasmon energies in curved geometries under the assumption that the separation is small compared with the radius of curvature. In particular for a sphere dimer, we model the evolution of the plasmon amplitude ψ through the Helmholz equation $(\nabla^2 + k_{\parallel}^2)\psi = 0$, where $k_{\parallel}$ depends on the surface-to-surface separation at a radial distance r away from the axis of symmetry. Starting from a finite amplitude at $r = 0$, we obtain the $r \to \infty$ limit (*i.e.*, in a region where $k_{\parallel}$ does no longer depend on r because the separation is too large) upon numerical integration and compare it with a combination of Hankel functions $H_0^{(1)}$ and $H_0^{(2)}$. The plasmon energies result from the condition that the coefficient of $H_0^{(2)}$ is zero (*i.e.*, no incoming waves). The results of this procedure are shown in Figure 5 for sharp (black curves) and smooth (red curves) interfaces using both

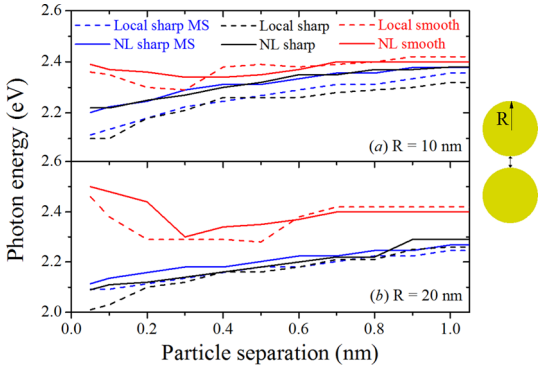

Figure 5. Gap plasmons in a gold sphere dimer. We calculate the dependence of the gap plasmon energy on surface-to-surface separation for spheres of 10 and 20 nm radius. Multiple-scattering (MS) theory for a sharp density profile (blue) is compared with an approximate method based upon the plasmons in the planar gap geometry for either sharp (black) or smooth (red) density profiles. Local and nonlocal results are represented as dashed and solid curves, respectively.

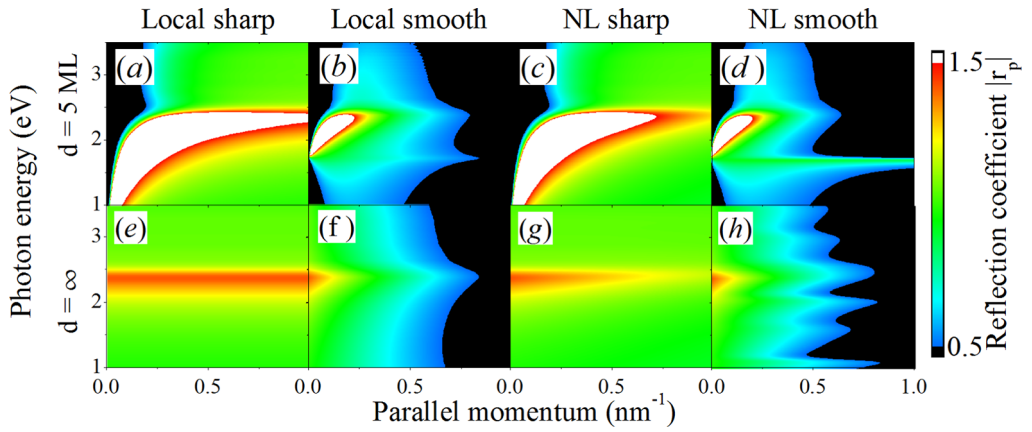

Figure 6. Plasmon dispersion in thin gold films. We compare the momentum and energy dependence of the reflection coefficient $|r_p|$ for a film consisting of five (111) atomic layers (MLs) (a–d) with the reflection from a semi-infinite surface (e–h) using different models for the response (see upper labels).

local (dashed curves) and nonlocal (solid curves) models for the response. We further show the gap plasmons obtained from a more rigorous multiple-scattering (MS) procedure, which is so far only applicable to sharp interfaces.[27] This comparison corroborates the validity of the approximate Helmholz equation method, which agrees reasonably well with the MS results. Overall, we observe again that the effect of smoothness in the interface is large compared with spatial dispersion. Essentially, the redshift produced by interparticle interaction is reduced due to the smoothness in the profile, in agreement with experiments.[11−13]

Plasmons in Ultrathin Films. For a thin gold film consisting of only a few atomic layers (see Figure 6a–d, and Figures S9 and S10 in the SI), we observe once more a dominant effect of the smooth density profile compared with finite hydrodynamic pressure. The latter produces just a small intensity reduction and blue shift of the dominant plasmon band, which strongly redshifts for decreasing $k_\parallel$ down to zero energy in both local and NL sharp models. In contrast, this feature only survives at $k_\parallel d < 3$ for smooth profiles, it is blue-shifted with respect to the sharp profiles, and it is saturated at a finite energy in the $k_\parallel \to 0$ limit. For a thickness $d \approx 1.2$ nm (*i.e.*, 5 atomic layers), this saturation occurs at ~1.8 eV. Interestingly, a dispersionless feature appears at this energy, which is more pronounced in the NL smooth model compared to the local smooth model.

CONCLUSIONS AND OUTLOOK

In summary, we provide a fast method to simulate the optical properties of metal surfaces that is applicable to small distances and gaps between metals down to the subnanometer scale. In this method, the hydrodynamic model is extended to account for the smooth variation of the electron density profile at the surface. The latter is obtained from well-established density-functional theory within the jellium model approach.[14] The smooth density profile turns out to be of critical importance for quantitatively predicting the surface optical response. Our results are consistent with quantum theory and experiments of gap plasmons,[7,12,13,17] and in particular, they reproduce the small plasmon redshift observed near touching compared with both local and nonlocal hydrodynamic theories for abrupt interfaces.

The smoothness of the density profile is a dominant effect when compared with spatial dispersion introduced through realistic values of the hydrodynamic pressure parameter β. We understand that a fit of β in an abrupt surface model is only providing a phenomenological description of experiment,[12] but obviously ignores electron spill-out effects. In fact, spatial dispersion alone with β obtained from the bulk RPA response predicts a plasmon blue shift that is too large in the single interface and too small in the gap geometry, with the smooth profile providing a dominant correction in the direction of the experiments. It should be noted that a recent extension of the nonlocal hydrodynamic model also explains the experimental observations using abrupt interfaces and introducing a contribution from electron diffusion.[31] Surprisingly, without diffusion, local smooth and nonlocal smooth models yield similar results in all geometries under consideration.

The present approach can be easily extended to other curved geometries, where it should find application to predict the optical response and the interaction of molecules in close proximity to metal surfaces. This is in contrast to quantum analyses based on first-principles, where the problem of finding first the electron wave functions and then the self-consistent susceptibility is unsurmountable with our current computational capabilities when the size of the system exceeds a few nanometers. There is a clear need to investigate hybrid methods combining the power of the present hydrodynamic approach for large systems with the accuracy of first-principles methods for small

subsystems (or even as a source of fitted spill-out profiles and hydrodynamic parameters). We thus hope that this work contributes to the ongoing effort of understanding the optical behavior of arbitrarily complex nanostructures that involve critical subnanometer elements.

METHODS

Hydrodynamic Model for One-Dimensional Density Profiles. In this work, we focus on surfaces, gaps, and thin films comprising smooth planar interfaces that are homogeneous along planes normal to the z direction, so that all physical quantities can be expressed as a sum over wave vector components $\mathbf{k}_\parallel$ and the dependence on $\mathbf{R} = (x,y)$ comes through an implicitly understood $\exp(i\mathbf{k}_\parallel \cdot \mathbf{R})$ factor. This allows us to make the substitution $\nabla \rightarrow (i\mathbf{k}_\parallel, \partial_z)$. Now, eliminating the current from eq 2, we find from eqs 3 and 4 the self-consistent scalar equations

$$(\beta^2\rho^{\text{ind}})'' + q^2\beta^2\rho^{\text{ind}} - \frac{3}{2}[\rho^{\text{ind}}(\beta^2)']' = \frac{-e^2}{m_e}\left(\frac{n_0}{\epsilon_b}\right)'(\epsilon_b\phi') \quad (5)$$

$$\phi'' - k_\parallel^2\phi + \frac{\epsilon_b'}{\epsilon_b}\phi' = -\frac{4\pi}{\epsilon_b}\rho^{\text{ind}} \quad (6)$$

where the prime denotes differentiation with respect to z, and we have defined

$$q = \sqrt{(\epsilon_\perp/\beta^2\epsilon_b)\omega(\omega + i\gamma) - k_\parallel^2}$$

with $Im\{q\} > 0$. Interestingly, this expression involves the local transversal permittivity

$$\epsilon_\perp = \epsilon_b - \frac{\omega_p^2}{\omega(\omega + i\gamma)} \quad (7)$$

which takes a Drude form with local plasma frequency $\omega_p = (4\pi e^2 n_0/m_e)^{1/2}$, defined in terms of the z-dependent unperturbed electron density n_0. The complex background permittivity ϵ_b is chosen such that eq 7 agrees with the measured bulk dielectric function (see Figure S1 in the SI).

Our strategy to model a nonlocal medium that is inhomogeneous along the z direction consists in describing it as a concatenation of uniform layers of vanishing thickness. We thus need to have the solution of the above equations for nonlocal homogeneous media, as well as the reflection and transmission at sharp interfaces separating the layers.

Nonlocal Homogeneous Medium. The right-hand side of eq 5 and the last term in the left-hand side vanish in a homogeneous medium (say medium j), so that we can write the induced density as a combination of two waves propagating toward positive and negative z directions,

$$\rho^{\text{ind}} = \mathcal{A}_1^{(j)} e^{iq^{(j)}z} + \mathcal{A}_2^{(j)} e^{-iq^{(j)}z} \quad (8)$$

where the coefficients $\mathcal{A}_l^{(j)}$ are determined from the boundary conditions (see below). Inserting eq 8 into eq 6, we can write the potential as

$$\phi = \mathcal{A}_3^{(j)} e^{-k_\parallel z} + \mathcal{A}_4^{(j)} e^{k_\parallel z} + B^{(j)}\rho^{\text{ind}} \quad (9)$$

where

$$B^{(j)} = \frac{4\pi(\beta^{(j)})^2}{\epsilon_\perp^{(j)}\omega(\omega + i\gamma)} \quad (10)$$

Obviously, these solutions depend on the properties of medium j through n_0 and ϵ_b, which act as input parameters that determine other derived quanties such as β, q, and $\epsilon_\perp$.

Transfer Matrix Approach. We intend to find a transfer matrix $\mathbf{T}^{(j,j-1)}$ that relates the coefficients $\mathcal{A}_l^{(j)}$ in medium j to those in medium $j-1$ (see Figure 7c),

$$\mathcal{A}^{(j)} = \mathbf{T}^{(j,j-1)} \cdot \mathcal{A}^{(j-1)} \quad (11)$$

The two media are separated by a sharp interface, as illustrated in Figure 7c. Using eqs 8 and 9 with the origins of the exponentials defined at the interface, we find $\mathbf{M}^{(j)} \cdot \mathcal{A}^{(j)} = \mathbf{M}^{(j-1)} \cdot \mathcal{A}^{(j-1)}$, where the rows of the matrix

$$\mathbf{M}^{(j)} = \begin{pmatrix} B^{(j)} & B^{(j)} & 1 & 1 \\ iq^{(j)}\epsilon_b^{(j)}B^{(j)} & -iq^{(j)}\epsilon_b^{(j)}B^{(j)} & -\epsilon_b^{(j)}k_\parallel & \epsilon_b^{(j)}k_\parallel \\ 1/\beta^{(j)} & 1/\beta^{(j)} & 0 & 0 \\ -C^{(j)} & C^{(j)} & \frac{e^2}{m_e}k_\parallel n_0^{(j)} & -\frac{e^2}{m_e}k_\parallel n_0^{(j)} \end{pmatrix}$$

are extracted from ϕ, $\epsilon_b\partial\phi/\partial z$, ρ^{ind}/β, and j_z^{ind} (*i.e.*, the magnitudes that are continuous across the interface). The coefficient $B^{(j)}$ is given by eq 10, and we have further defined

$$C^{(j)} = iq^{(j)}(\beta^{(j)})^2\epsilon_b^{(j)}/\epsilon_\perp^{(j)}$$

When more interfaces are considered, it is convenient to choose the origins of the exponentials of eqs 8 and 9 at the right end of each homogeneous layer, so that the transfer matrix $\mathbf{T}^{(j,j-1)}$ in eq 11 must include the propagation across layer j of thickness Δz_j. We find

$$\mathbf{T}^{(j,j-1)} = \mathbf{P}^{(j)} \cdot \frac{1}{\mathbf{M}^{(j)}} \cdot \mathbf{M}^{(j-1)}$$

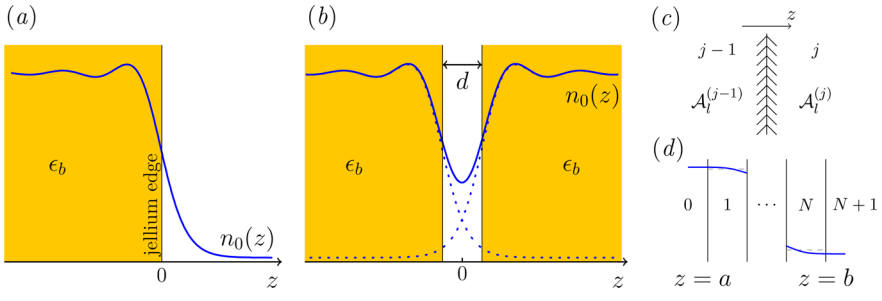

Figure 7. Illustration of smooth surface electron density profiles and discretization method used to simulate their optical response. (a) Density profile for a planar gold surface (blue curve, taken from ref 44) relative to the jellium edge ($z = 0$). (b) Same as (a) for a gap of jellium-to-jellium distance d. (c,d) Discretization along the normal direction z and relevant parameters used in the numerical procedure.

where

$$\mathbf{P}^{(j)} = \begin{pmatrix} e^{iq^{(j)}\Delta z_j} & 0 & 0 & 0 \\ 0 & e^{-iq^{(j)}\Delta z_j} & 0 & 0 \\ 0 & 0 & e^{-k_{\parallel}\Delta z_j} & 0 \\ 0 & 0 & 0 & e^{k_{\parallel}\Delta z_j} \end{pmatrix}$$

Finally, for a smooth interface described by N films of media $j = 1, ..., N$, with medium $j = 0$ ($j = N + 1$) to the left (right) of the interface (see Figure 7d), the full transfer matrix reduces to

$$\mathbf{T} = \frac{1}{\mathbf{M}^{(N+1)}} \cdot \mathbf{M}^{(N)} \cdot \mathbf{T}^{(N,N-1)} \ldots \mathbf{T}^{(1,0)}$$

and the propagation across the full interface is expressed as

$$\mathscr{A}^{(N+1)} = \mathbf{T} \cdot \mathscr{A}^{(0)} \tag{12}$$

Obviously, the z origin of the exponentials in medium $N + 1$ must be reset to the left end of that medium. Matrix $\mathbf{T}$ propagates the coefficients of eqs 8 and 9 from position $z = a$ at the 0|1 interface to position $z = b$ at the $N|N + 1$ interface (see Figure 7d).

In our simulations, we obtain full convergence with increasing N by setting all thicknesses $\Delta z_j \sim 0.001$ nm. For a metal surface, only the varying part of the density profile near the interface has to be computed in this way. Propagation in the bulk of the material is simply described by eqs 8 and 9. Incidentally, the last interface with a local medium (*e.g.*, vacuum) has to be taken with care, and we obtain converged results in the limit when the local medium is simply approached by setting $n_0 \to 0$.

Calculation of Reflection Coefficients. We are now equipped to obtain the dispersion relation for plasmons bound to planar structures, including the effect of smooth electron-density profiles (*e.g.*, a single metal-dielectric planar interface, a thin metal film, or a dielectric gap buried in metal). We consider positions $z = a$ and $z = b$ placed in the homogeneous regions on either side of the structure, separated by a smooth density profile (see Figure 7b). Similar to Otto's configuration,[55] surface plasmons can be excited by an incident evanescent wave. We thus take a unit potential incident from the left, as well as its reflection at the planar structure, $\phi = e^{-k_0(z-a)} - r_p e^{k_0(z-a)}$, where r_p is the reflection coefficient. Surface plasmons are signaled by the poles of r_p, which yield a reflected component even without an external source (*i.e.*, they are evanescent waves confined to the surface). This allows us to write the coefficients in medium $j = 0$ ($z < a$ region) as

$$\mathscr{A}^{(0)} = \begin{pmatrix} 0 \\ \mathscr{A}_2^{(0)} \\ 1 \\ -r_p \end{pmatrix} \tag{13}$$

where we disregard incident density components, but we still maintain a reflected density amplitude $\mathscr{A}_2^{(0)}$. Incidentally, the latter multiplies a vanishing exponential in the local-medium side of an interface, according to eq 8. The transmitted coefficients across the interface must only have components propagating toward the right in the $z > b$ region; that is,

$$\mathscr{A}^{(N+1)} = \begin{pmatrix} \mathscr{A}_1^{(N+1)} \\ 0 \\ \mathscr{A}_3^{(N+1)} \\ 0 \end{pmatrix} \tag{14}$$

Inserting eqs 13 and 14 into eq 12, we find

$$r_p = -\frac{T_{22}T_{43} - T_{42}T_{23}}{T_{42}T_{24} - T_{22}T_{44}} \tag{15}$$

Finally, the maxima of $|r_p|$ as a function of ω yield the plasmon frequency for each parallel wave vector $k_{\parallel}$.

Calculation of the LDOS. We obtain the LDOS along the surface normal (z direction) from the self-induced field at the position of a unit dipole[56]

$$\rho_{\text{ind}}^{\text{LDOS}} = (1/2\pi)\int_0^{\infty} dk_{\parallel}\, k_{\parallel}\, \rho_{k_{\parallel}}(\omega)$$

where

$$\rho_{k_{\parallel}}(\omega) = \frac{1}{2\pi^2\omega} Im\{E_z^{\text{ind}}(k_{\parallel}, \omega)\} \tag{16}$$

is the $k_{\parallel}$-resolved LDOS. The field is in turn calculated with the methods described above. At a position z_d sufficiently far from the surface as to consider the electron spill-out negligible, eq 16 reduces to

$$\rho_{k_{\parallel}}(\omega) = \frac{k_{\parallel}}{\pi\omega} e^{-2k_{\parallel}|z_d|} Im\{r_p\} \tag{17}$$

where r_p is the reflection coefficient defined in eq 15. For a gap, multiple reflections at the surfaces permit expressing the LDOS using a Fabry–Pérot-like model when the separation is so large that the density becomes negligible at the gap center where the LDOS is evaluated. We have verified that this model agrees well at large separations with the full solution of the hydrodynamic equations for the entire gap using the $k_{\parallel}$-resolved field from a dipole as input (see Figure S7 in the SI).

Conflict of Interest: The authors declare no competing financial interest.

Acknowledgment. C.D. acknowledges a FPU fellowship from the Spanish Ministerio de Educación.

Supporting Information Available: We provide details of the dependence of the optical response on various parameters. We further explore the evolution from smooth to abrupt interfaces as the density profile is sharpened, as well as the transition from nonlocal to local smooth-profile theories by reducing the value of the hydrodynamic pressure parameter β. Further simulations for thin films and gaps are also offered. This material is available free of charge *via* the Internet at http://pubs.acs.org.

Note Added after ASAP Publication: This paper published ASAP on August 25, 2014. Changes were made to equations in the Calculation of Reflection Coefficients section and the revised version was reposted on August 27, 2014.

REFERENCES AND NOTES

1. Halas, N. J.; Lal, S.; Chang, W.; Link, S.; Nordlander, P. Plasmons in Strongly Coupled Metallic Nanostructures. *Chem. Rev.* **2011**, *111*, 3913–3961.
2. Álvarez-Puebla, R. A.; Liz-Marzán, L. M.; García de Abajo, F. J. Light Concentration at the Nanometer Scale. *J. Phys. Chem. Lett.* **2010**, *1*, 2428–2434.
3. Liz-Marzán, L. M. Tailoring Surface Plasmon through the Morphology and Assembly of Metal Nanoparticles. *Langmuir* **2006**, *22*, 32–41.
4. Anker, J. N.; Hall, W. P.; Lyandres, O.; Shah, N. C.; Zhao, J.; Van Duyne, R. P. Biosensing with Plasmonic Nanosensors. *Nat. Mater.* **2008**, *7*, 442–453.
5. Xu, H.; Bjerneld, E. J.; Käll, M.; Börjesson, L. Spectroscopy of Single Hemoglobin Molecules by Surface Enhanced Raman Scattering. *Phys. Rev. Lett.* **1999**, *83*, 4357–4360.
6. Danckwerts, M.; Novotny, L. Optical Frequency Mixing at Coupled Gold Nanoparticles. *Phys. Rev. Lett.* **2007**, *98*, 026104.
7. Savage, K. J.; Hawkeye, M. M.; Esteban, R.; Borisov, A. G.; Aizpurua, J.; Baumberg, J. J. Revealing the Quantum Regime in Tunnelling Plasmonics. *Nature* **2012**, *491*, 574–577.
8. Pazos-Perez, N.; Wagner, C. S.; Romo-Herrera, J. M.; Liz-Marzán, L. M.; García de Abajo, F. J.; Wittemann, A.; Fery, A.; Alvarez-Puebla, R. A. Organized Plasmonic Clusters with High Coordination Number and Extraordinary Enhancement in Surface-Enhanced Raman Scattering (SERS). *Ang. Chem. Int. Ed.* **2012**, *51*, 12688–12693.
9. Rodríguez-Lorenzo, L.; Álvarez-Puebla, R. A.; Pastoriza-Santos, I.; Mazzucco, S.; Stéphan, O.; Kociak, M.; Liz-Marzán, L. M.; García de Abajo, F. J. Zeptomol Detection through Controlled Ultrasensitive Surface-Enhanced Raman Scattering. *J. Am. Chem. Soc.* **2009**, *131*, 4616–4618.

10. Politano, A.; Formoso, V.; Chiarello, G. Dispersion and Damping of Gold Surface Plasmon. *Plasmonics* **2008**, *3*, 165–170.
11. Scholl, J. A.; Koh, A. L.; Dionne, J. A. Quantum Plasmon Resonances of Individual Metallic Nanoparticles. *Nature* **2012**, *483*, 421–428.
12. Cirací, C.; Hill, R. T.; Mock, J. J.; Urzhumov, Y.; Fernández-Domnguez, A. I.; Maier, S. A.; Pendry, J. B.; Chilkoti, A.; Smith, D. R. Probing the Ultimate Limits of Plasmonic Enhancement. *Science* **2012**, *337*, 1072–1074.
13. Raza, S.; Stenger, N.; Kadkhodazadeh, S.; Fischer, S. V.; Kostesha, N.; Jauho, A.-P.; Burrows, A.; Wubs, M.; Mortensen, N. A. Blueshift of the Surface Plasmon Resonance in Silver Nanoparticles Studied with EELS. *Nanophotonics* **2013**, *2*, 131.
14. Liebsch, A. Surface-Plasmon Dispersion and Size Dependence of Mie Resonance: Silver *versus* Simple Metals. *Phys. Rev. B: Condens. Matter Mater. Phys.* **1993**, *48*, 11317–11328.
15. Zuloaga, J.; Prodan, E.; Nordlander, P. Quantum Description of the Plasmon Resonances of a Nanoparticle Dimer. *Nano Lett.* **2009**, *9*, 887–891.
16. Zuloaga, J.; Prodan, E.; Nordlander, P. Quantum Plasmonics: Optical Properties and Tunability of Metallic Nanorods. *ACS Nano* **2010**, *4*, 5269–5276.
17. Esteban, R.; Borisov, A. G.; Nordlander, P.; Aizpurua, J. Bridging Quantum and Classical Plasmonics with a Quantum-Corrected Model. *Nat. Commun.* **2012**, *3*, 825.
18. Ford, G. W.; Weber, W. H. Electromagnetic Interactions of Molecules with Metal Surfaces. *Phys. Rep.* **1984**, *113*, 195–287.
19. Ritchie, R. H.; Marusak, A. L. The Surface Plasmon Dispersion Relation for an Electron Gas. *Surf. Sci.* **1966**, *4*, 234–240.
20. Kliewer, K. L.; Fuchs, R. Lindhard Dielectric Functions with a Finite Electron Lifetime. *Phys. Rev.* **1969**, *181*, 552–558.
21. Fuchs, R.; Claro, F. Multipolar Response of Small Metallic Spheres: Nonlocal Theory. *Phys. Rev. B: Condens. Matter Mater. Phys.* **1987**, *35*, 3722–3727.
22. Rojas, R.; Claro, F.; Fuchs, R. Nonlocal Response of a Small Coated Sphere. *Phys. Rev. B: Condens. Matter Mater. Phys.* **1988**, *37*, 6799–6807.
23. García de Abajo, F. J. Nonlocal Effects in the Plasmons of Strongly Interacting Nanoparticles, Dimers, and Waveguides. *J. Phys. Chem. C* **2008**, *112*, 17983–17987.
24. García de Abajo, F. J. Optical Excitations in Electron Microscopy. *Rev. Mod. Phys.* **2010**, *82*, 209–275.
25. Bloch, F. Bremsvermögen von Atomen mit mehreren Elektronen. *Z. Phys.* **1933**, *81*, 363–376.
26. Boardman, A.; Ruppin, R. The Boundary Conditions between Spatially Dispersive Media. *Surf. Sci.* **1981**, *112*, 153–167.
27. David, C.; García de Abajo, F. J. Spatial Nonlocality in the Optical Response of Metal Nanoparticles. *J. Phys. Chem. C* **2011**, *115*, 19470–19475.
28. McMahon, J. M.; Gray, S. K.; Schatz, G. C. Calculating Nonlocal Optical Properties of Structures with Arbitrary Shape. *Phys. Rev. B: Condens. Matter Mater. Phys.* **2010**, *82*, 035423.
29. Raza, S.; Toscano, G.; Jauho, A.-P.; Wubs, M.; Mortensen, N. A. Unusual Resonances in Nanoplasmonic Structures Due to Nonlocal Response. *Phys. Rev. B: Condens. Matter Mater. Phys.* **2011**, *84*, 121412.
30. Kreibig, U.; Vollmer, M. *Optical Properties of Metal Clusters*; Springer-Verlag: Berlin, 1995.
31. Mortensen, N. A.; Raza, S.; Wubs, M.; Søndergaard, T.; Bozhevolnyi, S. I. A Generalized Non-Local Optical Response Theory for Plasmonic Nanostructures. *Nat. Commun.* **2014**, *5*, 3809.
32. Lassiter, J. B.; Aizpurua, J.; Hernandez, L. I.; Brandl, D. W.; Romero, I.; Lal, S.; Hafner, J. H.; Nordlander, P.; Halas, N. J. Close Encounters between Two Nanoshells. *Nano Lett.* **2008**, *8*, 1212–1218.
33. Dasgupta, B. B.; Fuchs, R. Polarizability of a Small Sphere Including Nonlocal Effects. *Phys. Rev. B: Condens. Matter Mater. Phys.* **1981**, *24*, 554–561.
34. Ruppin, R. Optical Properties of Spatially Dispersive Dielectric Spheres. *J. Opt. Soc. Am.* **1981**, *71*, 755–758.
35. Ruppin, R. Optical Absorption by a Small Sphere above a Substrate with Inclusion of Nonlocal Effects. *Phys. Rev. B: Condens. Matter Mater. Phys.* **1992**, *45*, 11209–11215.
36. Aizpurua, J.; Rivacoba, A. Nonlocal Effects in the Plasmons of Nanowires and Nanocavities Excited by Fast Electron Beams. *Phys. Rev. B: Condens. Matter Mater. Phys.* **2008**, *78*, 035404.
37. McMahon, J. M.; Gray, S. K.; Schatz, G. C. Nonlocal Optical Response of Metal Nanostructures with Arbitrary Shape. *Phys. Rev. Lett.* **2009**, *103*, 097403.
38. McMahon, J. M.; Gray, S. K.; Schatz, G. C. Optical Properties of Nanowire Dimers with a Spatially Nonlocal Dielectric Function. *Nano Lett.* **2010**, *10*, 3473–3481.
39. Toscano, G.; Raza, S.; Jauho, A.-P.; Mortensen, N. A.; Wubs, M. Modified Field Enhancement and Extinction by Plasmonic Nanowire Dimers Due to Nonlocal Response. *Opt. Express* **2012**, *20*, 4176–4188.
40. Öztürk, Z. F.; Xiao, S.; Yan, M.; Wubs, M.; Jauho, A.-P.; Mortensen, N. A. Field Enhancement at Metallic Interfaces Due to Quantum Confinement. *J. Nanophoton* **2011**, *5*, 051602.
41. Ruppin, R. Effect of Non-locality on Nanofocusing of Surface Plasmon Field Intensity in a Conical Tip. *Phys. Lett. A* **2005**, *340*, 299–302.
42. Wiener, A.; Fernández-Domínguez, A. I.; Horsfield, A. P.; Pendry, J. B.; Maier, S. A. Nonlocal Effects in the Nanofocusing Performance of Plasmonic Tips. *Nano Lett.* **2012**, *12*, 865–871.
43. Fernández-Domínguez, A. I.; Wiener, A.; García-Vidal, F. J.; Maier, S. A.; Pendry, J. B. Transformation-Optics Description of Nonlocal Effects in Plasmonic Nanostructures. *Phys. Rev. Lett.* **2012**, *108*, 106802.
44. Lang, N. D.; Kohn, W. Theory of Metal Surfaces: Charge Density and Surface Energy. *Phys. Rev. B: Solid State* **1970**, *1*, 4555–4568.
45. Eguiluz, A.; Ying, S. C.; Quinn, J. J. Influence of the Electron Density Profile on Surface Plasmons in a Hydrodynamic Model. *Phys. Rev. B: Solid State* **1975**, *11*, 2118–2121.
46. Sipe, J. E.; So, V. C. Y.; Fukui, M.; Stegeman, G. I. Analysis of Second-Harmonic Generation at Metal Surfaces. *Phys. Rev. B: Condens. Matter Mater. Phys.* **1980**, *21*, 4389–4402.
47. Huang, K. *Statistical Mechanics*; Wiley: New York, 1963.
48. Pines, D.; Bohm, D. A Collective Description of Electron Interactions: II. Collective *vs* Individual Particle Aspects of the Interactions. *Phys. Rev.* **1952**, *85*, 338–353.
49. Ritchie, R. H. Plasma Losses by Fast Electrons in Thin Films. *Phys. Rev.* **1957**, *106*, 874–881.
50. Johnson, P. B.; Christy, R. W. Optical Constants of the Noble Metals. *Phys. Rev. B: Solid State* **1972**, *6*, 4370–4379.
51. Chiarello, G.; Formoso, V.; Santaniello, A.; Colavita, E.; Papagno, L. Surface-Plasmon Dispersion and Multipole Surface Plasmons in Al(111). *Phys. Rev. B: Condens. Matter Mater. Phys.* **2000**, *62*, 12676–12679.
52. Eriksson, H. G.; R.Karlsson, B.; Wijewardena, K. A. I. L. Oscillatory Polarization Potential Induced at a Surface by a Penetrating Charge. *Phys. Rev. B: Condens. Matter Mater. Phys.* **1985**, *31*, 843–849.
53. Fussell, D. P.; McPhedran, R. C.; Martijn de Sterke, C. Three-Dimensional Green's Tensor, Local Density of States, and Spontaneous Emission in Finite Two-Dimensional Photonic Crystals composed of Cylinders. *Phys. Rev. E: Stat., Nonlinear, Soft Matter Phys.* **2004**, *70*, 066608.
54. Blanco, L. A.; García de Abajo, F. J. Spontaneous Light Emission in Complex Nanostructures. *Phys. Rev. B: Condens. Matter Mater. Phys.* **2004**, *69*, 205414.
55. Otto, A. Theory of Plasmon Excitation in Thin Films by Electrons of Non-Normal Incidence. *Phys. Status Solidi* **1967**, *22*, 401–406.
56. Novotny, L.; Hecht, B. *Principles of Nano-Optics*; Cambridge University Press: New York, 2006.